Seasonal freeze-thaw cycles and permafrost degradation on Mt. Zugspitze (German/Austrian Alps) revealed by single-station seismic monitoring

Fabian Lindner[1], Joachim Wassermann[2], and Heiner Igel[3]

[1]LMU Munich
[2]Ludwig-Maximilians- University, Munich
[3]Geophysics Section

November 23, 2022

Abstract

Thawing of mountain permafrost in response to rising temperatures degrades the stability of rock walls and thereby affects infrastructure integrity in Alpine terrain. In this study, we use 15 years of passive seismic data from a single station deployed near a known permafrost body on Mt. Zugspitze (Germany), to monitor freeze-thaw processes. The recordings reveal a persistent cultural seismic noise source, which we utilize to compute single-station cross-correlations and extract relative seismic velocity changes. We find that parts of the cross-correlations show seasonal velocity variations (3% peak-to-peak amplitude) and a long-term velocity decrease (0.1%/yr). Comparison with meteorological data and a previous electrical resistivity tomography study suggests that these velocity changes are caused by active-layer freeze-thaw cycles and by permafrost degradation, respectively. The results demonstrate the potential of passive seismology for permafrost monitoring and suggest that denser instrumentation will provide detailed spatio-temporal insights on permafrost dynamics in future studies.

Seasonal freeze-thaw cycles and permafrost degradation on Mt. Zugspitze (German/Austrian Alps) revealed by single-station seismic monitoring

Fabian Lindner[1], Joachim Wassermann[1], Heiner Igel[1]

[1]Department of Earth and Environmental Sciences, LMU Munich, Theresienstraße 41, 80333, Munich, Germany

Key Points:

- We use a single seismic station deployed near a permafrost body on Mt. Zugspitze (Germany) to monitor freeze-thaw processes over 15 years
- Cross-correlations between the sensor components reveal seasonal velocity change cycles and a long-term velocity decrease
- The changes are due to seasonal freeze-thaw cycles and permafrost degradation, suggesting seismology as effective permafrost monitoring tool

Corresponding author: F. Lindner, `flindner@geophysik.uni-muenchen.de`

Abstract

Thawing of mountain permafrost in response to rising temperatures degrades the stability of rock walls and thereby affects infrastructure integrity in Alpine terrain. In this study, we use 15 years of passive seismic data from a single station deployed near a known permafrost body on Mt. Zugspitze (Germany), to monitor freeze-thaw processes. The recordings reveal a persistent cultural seismic noise source, which we utilize to compute single-station cross-correlations and extract relative seismic velocity changes. We find that parts of the cross-correlations show seasonal velocity variations (≈3% peak-to-peak amplitude) and a long-term velocity decrease (≈0.1%/yr). Comparison with meteorological data and a previous electrical resistivity tomography study suggests that these velocity changes are caused by active-layer freeze-thaw cycles and by permafrost degradation, respectively. The results demonstrate the potential of passive seismology for permafrost monitoring and suggest that denser instrumentation will provide detailed spatio-temporal insights on permafrost dynamics in future studies.

Plain Language Summary

Climate change causes permafrost (year-round frozen rock) warming and thawing, which destabilizes rock slopes and thus constitutes a hazard potential. However, unlike glacier retreat, permafrost thawing cannot be directly observed from the surface and requires special imaging techniques for monitoring. Here, we use seismic waves generated by cable cars and other man-made infrastructure to probe permafrost on Mt. Zugspitze (Germany) and track temporal changes over the past 15 years. Results from a single seismic station show that the seismic wave propagation velocity in the rock is subject to seasonal variations (difference between late winter and late summer of up to 3%) and a long-term decrease of roughly 0.1% per year. As the seismic velocity is generally higher in frozen rock compared to unfrozen rock, the seasonal changes can be well explained by seasonal thaw and refreeze, and the long-term changes by ongoing permafrost thawing. Because passive seismology is labour and cost effective compared to common techniques requiring active signal excitation, seismology constitutes a promising new approach for continuous long-term permafrost monitoring.

1 Introduction

Permafrost refers to the perennially frozen ground and underlies more than 20% of the Northern Hemisphere land area (Zhang et al., 2008) including high-elevation areas in the European Alps. With rising atmospheric temperatures, permafrost warming and thawing are observed (Beniston et al., 2018; Biskaborn et al., 2019; Mollaret et al., 2019), which affects the rock mechanical properties and degrades the stability of slopes (Davies et al., 2001; Mellor, 1973; Haeberli et al., 2010; Krautblatter et al., 2013). As a consequence, climate change is expected to result in an increase in rock detachments in permafrost areas (Gruber & Haeberli, 2007), already observable by a correlation between rockfall activity and temperatures (Ravanel et al., 2017; Huggel et al., 2012; Gruber et al., 2004a). In addition, individual larger, partly catastrophic rock detachments from permafrost affected mountains have been documented in recent years (Walter et al., 2020; Phillips et al., 2017; Pirulli, 2009). This highlights the hazard potential of permafrost degradation for infrastructure and settlements, and thus the importance to understand and monitor the spatio-temporal evolution of mountain permafrost.

The occurrence of permafrost can be delineated to areas with long-term mean annual air temperatures below the freezing point, with colder temperatures favoring larger volumes of permafrost (Haeberli et al., 2010). Yet, the site specific permafrost conditions are affected by topography (Noetzli & Gruber, 2009), the local solar radiation conditions (Hoelzle et al., 2001), and the exposure to the atmosphere. Steep rock walls are usually free of debris, which promotes a rapid response to changes in the thermal forcing (Gruber et al., 2004b), whereas debris and snow cover have an insulating effect. In addition to the thermal forcing through heat conduction, advective heat transfer through (melt)water percolation can rapidly develop deep thaw corridors in fractured rocks (Kane et al., 2001). The complex interplay between numerous processes results in a heterogeneous three-dimensional distribution of mountain permafrost in lenses rather than layers (Krautblatter & Hauck, 2007).

Permafrost bodies can be monitored directly through temperature logging in boreholes (Haeberli et al., 1998; Beniston et al., 2018) or through surface-based geophysical imaging techniques including electrical resistivity tomography (ERT) and active seismics (Kneisel et al., 2008; Hauck, 2013). These methods can be used to differentiate between frozen and unfrozen ground (Hauck, 2002; Timur, 1968; King, 1977; Harris & Cook, 1986; Kneisel et al., 2008), or to even infer the temperature distribution in the case of ERT (Krautblatter et al., 2010; Scandroglio, Draebing, et al., 2021). While boreholes allow continuous permafrost monitoring, their wider applicability is limited by the logistics and costs involved. In contrast, active geophysical imaging techniques offer more flexibility but must be applied repeatedly to obtain temporal resolution. This remains challenging, as automatic acquisition in harsh Alpine terrain is difficult and manual acquisition e.g. on a monthly basis (Mollaret et al., 2019) is laborious.

To circumvent these limitations, passive seismic methods have been recently explored for permafrost monitoring. Applying ambient-noise based seismic interferometry, i.e. extracting repeatedly the seismic impulse response between pairs of seismic stations, James et al. (2019) find seasonal velocity changes of a few percent over the course of two years at a permafrost site in Alaska, which they attribute to active-layer freeze-thaw cycles. Using an array of continuously recording sensors, James et al. (2019) gain both spatial insights on the thaw depth and high temporal resolution such that they can track permafrost thawing caused by water infiltration from snow melt and rainfall events. Similar results are reported by Guillemot et al. (2020), who find seasonal changes in seismic velocities related to permafrost dynamics in the upper 10 m of a rock glacier. In this study, we investigate the potential of single-station passive seismology for continuous long-term permafrost monitoring. For this purpose, we apply seismic interferometry to a station deployed on the ridge of Mt. Zugspitze (Germany) close to a known permafrost lens. Data are available for the past 15 years and we extract seismic velocity change time series, which we compare to meteorological records and a previous ERT study.

2 Study site and seismic data

2.1 Mt. Zugspitze

Located at the German-Austrian border, Mt. Zugspitze (2962 m asl, WGS84 coordinates of the summit: 47.42119, 10.98634) is the highest peak in Germany. The summit area hosts three cable car stations and various other infrastructure including restaurants and broadcasting facilities (Fig. 1). Mt. Zugspitze is composed of triassic limestone (Wettersteinkalk) being weathered and fractured in the summit area and characterized by a subsurface cave drainage system established by Karst dissolution (Gude & Barsch, 2005; Krautblatter et al., 2010). Excavations for cable cars and other constructions revealed that the fractures are filled with up to decameter thick ice lenses and frozen loam (Körner & Ulrich, 1965; Ulrich & King, 1993). In prehistoric times, around 3700 years before present, a giant 0.3–0.4 km^3 rock slide occurred from the summit region, which is considered to have been triggered by permafrost degradation at the end of the Holocene climatic optimum (Jerz & von Poschinger, 1995).

In present times, permafrost is found in the north-facing rock, whereas the south-facing slopes are almost free of permafrost (Gude & Barsch, 2005; Nötzli et al., 2010). In 2007, a borehole was drilled beneath the summit, intersecting the crest entirely from

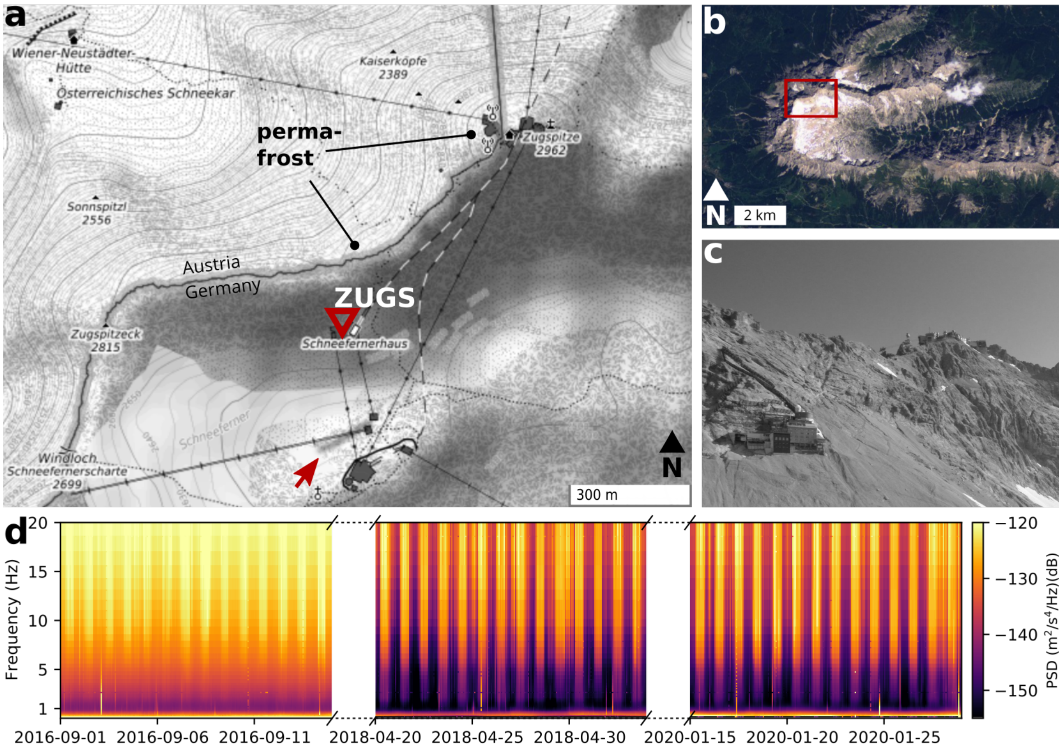

Figure 1. (a) Topographic map of the Zugspitze with the location of the the seismic station BW.ZUGS (red triangle) and two known permafrost areas. Black dotted lines are cable cars, black-white dashed lines are railway tunnels (map: OpenTopoMap). (b) Western part of the Wetterstein mountain range, the red rectangle shows the map extent from (a) (picture: Sentinel, 2017-06-26). (c) Photo of the permafrost affected ridge with the Schneefernerhaus (left) and the Zugspitze summit (right). View perspective is indicated by the red arrow in (a). (d) Vertical component spectrograms of station BW.ZUGS for two weeks in September 2016, April to May 2018, and January 2020 showing a persistent noise source during daytimes.

south to north on a length of 44 m. Temperature logging inside the borehole reveals permafrost temperatures down to about -4°C and seasonal thaw depths of 4.5 m and 1.5 m from the southern and northern side, respectively (Nötzli et al., 2010; Gallemann et al., 2017). Another permafrost body extends several tens of meters along the ridge north of the Schneefernerhaus research station (Fig. 1b) (Krautblatter et al., 2010), which is evident by perennial ice in a gallery intersecting the ridge. While the mean annual air temperature measured at the summit between 1901 and 2000 was -4.8°C, it was -3.7°C between 2001 and 2020, hence more than 1°C higher compared to the twentieth century. The increasing temperatures are reflected by permafrost warming and degradation visible in the borehole temperature logs beneath the summit (Gallemann et al., 2017).

2.2 Instrumentation

The Schneefernerhaus accommodates the permanent seismic station BW.ZUGS (Department of Earth and Environmental Sciences, Geophysical Observatory, LMU Munich, 2001) in a vault next to the rock face, which is operational since 2006 (Fig. 1). Initially, the station was equipped with a Mark L4-3D short-period seismometer (natural frequency of 1 Hz) and a Lennartz M24 digitizer. In August 2017, this setup was replaced by a Guralp CMG-3T broadband sensor and a Reftek RT130 digitizer. After a larger data gap starting in May 2018, the Guralp sensor was replaced by a Trillium Compact 120 s seismometer, which is operational since July 2019. The ground velocity output of all three sensors is sampled at 200 Hz. Spectrograms for the three different sensors at different times of the year (Fig. 1d) reveal a noise source being persistent over years with strong ground vibrations during the day, bound by the operation hours of the cable cars. Despite lower amplitudes at lower frequencies, the noise source is visible down to 2 Hz, where amplitudes are close to the self-noise level of the Mark L4-3D seismometer. Temporary deployments of two additional stations in February 2019 show that the noise amplitudes are stronger for installations closer to the summit area (not shown), suggesting the latter as excitation area.

3 Single-station monitoring and data processing

We utilize the single station to compute cross-correlations between the different sensor components (E, N, Z resulting in EN, EZ, NZ cross-correlations), which can be considered as impulse response retrieval for a source and a receiver being colocated (Hobiger et al., 2014; De Plaen et al., 2016; Yates et al., 2019). The single-station cross-correlations contain scattered and reflected waves with the EN component being sensitive to Rayleigh and Love waves, whereas the EZ and NZ components relying on vertical ground motions are not sensitive to Love waves. In addition to surface waves, the cross-correlations may also contain body waves reflected at depth including P-to S- and S-to P-converted phases (Hobiger et al., 2014; Becker & Knapmeyer-Endrun, 2019). We use the MSNoise package (Lecocq et al., 2014) to compute daily cross-correlations, which we form by stacking individual cross-correlations calculated from non-overlapping 30-minute windows and the frequency range of 0.1 to 25 Hz. The preprocessing includes the removal of the instrument response from the raw data, clipping of the seismograms at three times the root mean square amplitude, and spectral whitening to equalize the amplitude of all frequencies (Bensen et al., 2007) (all MSNoise processing parameters are provided in Table S1). Spectral whitening increases the robustness of the cross-correlations against noise source variability but cannot be applied for auto-correlations of individual channels as this results in a perfect delta pulse not carrying any information on the medium. The inhibited applicability of spectral whitening is the main disadvantage of auto-correlations (Hobiger et al., 2014). This is confirmed by this study, where the auto-correlation results appear to be similar to the single-station cross-correlations results, but noisier. We therefore focus on the single-station cross-correlations in this work.

To extract seismic velocity changes expressed as travel time changes, we compare the time-lapse cross-correlations against a reference cross-correlation. One common approach for this purpose is the moving-window cross-spectral (MWCS) technique (Clarke et al., 2011), where one employs a sliding window along the coda of bandpass filtered cross-correlations. The sliding window is used to determine the travel time shift δt as a function of the lag time t, averaged over the width of the sliding window and the frequency range of consideration. In a second step, one determines the slope $-\delta t/t$ through a linear regression, which is equal to the velocity change dv/v relative to the reference, if the latter affects the subsurface uniformly. Being related to the MWCS technique, we here explore the recently introduced wavelet cross-spectrum method (Mao et al., 2020), which also yields travel time shifts relative to the reference cross-correlation, but as a function of lag time and frequency f, i.e. $\delta t(t, f)$, hence with increased joint time-frequency resolution. This enables us to investigate specific parts of the cross-correlation. Here, we use the wavelet cross-spectrum implementation of the NoisePy package (Jiang & Denolle, 2020), employing a Morlet wavelet to compare 15 d cross-correlation stacks (calculated in a moving window with a step size of one day) against the reference. Regarding the reference, we consider two approaches. (1) We calculate the linear reference stack for the fixed reference period of 2017-09-01 to 2018-05-01 using all available daily cross-correlations. (2) As the seasonal freeze-thaw cycle associated with permafrost can cause such strong velocity changes relative to a fixed reference that the measurement of travel time shifts is affected by cycle skipping (James et al., 2017, 2019), we also consider a moving-reference type approach to mitigate this problem. To this end, we use 2016 as reference year, where we determine the seasonal travel time variations from adjacent 15 d stacks. Subsequently, for all other times, we determine the travel time variations as those of 2016 plus deviations to 2016 (e.g. $\delta t_{2017\text{-}03\text{-}17} = \delta t_{2016\text{-}03\text{-}17} + \delta t_{2017\text{-}03\text{-}17 vs 2016\text{-}03\text{-}17}$, see Text S1 for details).

4 Results

Active layer thaw and refreeze are governed by the temperature signal propagating into the rock with a period of one year. If cross-correlation coda waves sample freeze-thaw areas, we expect a periodic velocity change signal with the same period. We thus calculate the amplitude of the 365.25 d periodicity, $A_{LS}(365.25\,d)$, of all δt time series obtained from the wavelet cross-spectrum method relative to the fixed reference in the lag time of -5 s to 5 s and frequency range of 1 Hz to 20 Hz. Because Fourier analysis is hindered by data gaps in the δt time series, we employ the Lomb-Scargle periodogram (Lomb, 1976; Scargle, 1982), which enables us to compute power spectra at specific frequencies independent of the sample spacing. Fig. 2a-c shows $A_{LS}(365.25\,d)$ as a function of lag time and frequency, revealing that parts of the cross-correlations exhibit seasonal changes with a period of one year. This is further emphasized by the three δt time series (converted to $-\delta t/t$) representing specific lag-frequency combinations showing clear seasonal variations (Fig. 2d). Complementary to the individual $-\delta t/t$ curves, Fig. 2d also depicts the lag and frequency dependent $-\delta t/t$ measurements limits (horizontal dashed lines), beyond which cycle skipping occurs. While the two lower considered frequencies stay within these limits, the higher frequency $-\delta t/t$ curve (EZ, 9.92 Hz) is affected by cycle skipping as the variations are larger than the measurement limits.

To systematically investigate temporal changes, we consider the frequency dependence of $-\delta t/t$. Because we expect localized changes rather than uniform changes, we refrain from determining $-\delta t/t$ via linear regression, and instead determine the median from individual $-\delta t/t$ curves for each frequency bin. We restrict our analysis to the lag range bound by one and 15 times the respective period on the positive and negative branch of the cross-correlations (white dashed lines in Fig. 2a-c), hence using the same number of cycles independent of frequency. In addition, we only consider individual $-\delta t/t$ time series associated with a normalized Lomb-Scargle amplitude of at least 0.15, i.e. $A_{LS}(365.25\,d) \geq$

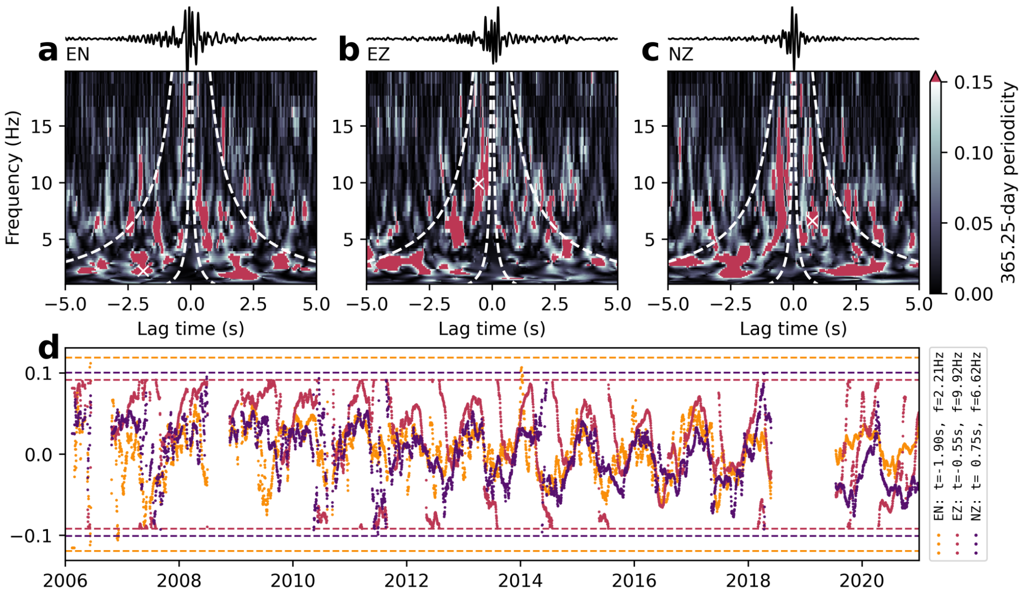

Figure 2. (a)-(c) EN, EZ, and NZ component cross-correlation reference stacks (seismograms, bandpass filtered 2-8 Hz) and 365.25 d periodicity of travel time shifts relative to the fixed reference (color maps). Red spots indicate combinations of lag time and frequency in the cross-correlations (joint time-frequency resolution achieved through wavelet-based cross-spectra) with a significant one-year period signal. White dashed lines indicate the frequency dependent lag times of one and 15 periods. (d) Travel time shifts (converted to $-\delta t/t$), for a lag-frequency combination of each component with high 365.25 d periodicity (white crosses in (a)-(c)). The horizontal dashed lines indicate the maximum $-\delta t/t$ measurement ranges for the three curves, outside of which cycle skipping occurs.

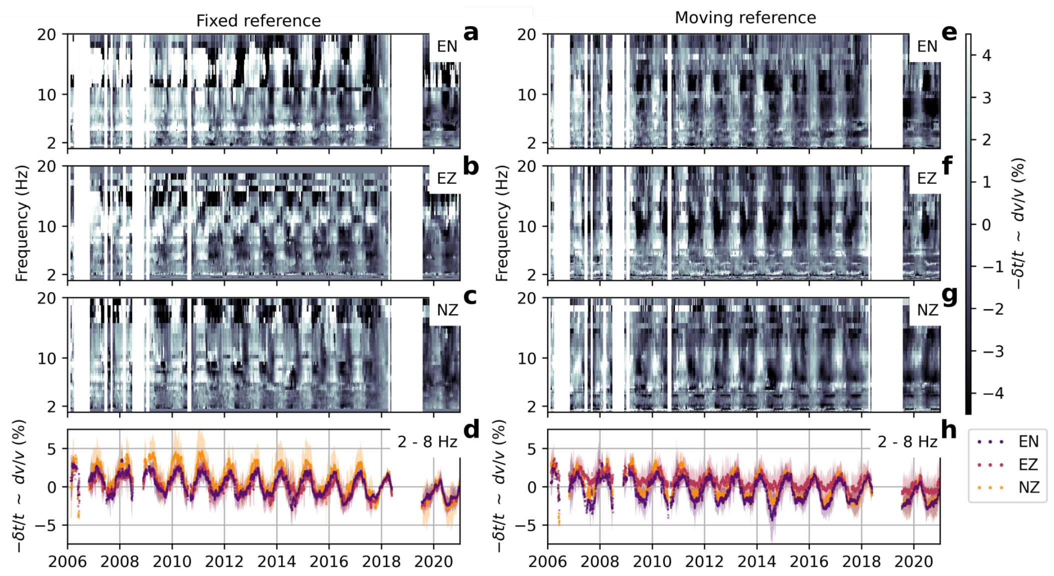

Figure 3. (a)-(c) Median travel time change $-\delta t/t$ for each frequency bin, computed from all individual time series associated with high 365.25 d periodicity ($A_{LS} \geq 0.15$) in the lag range bound by one and 15 periods. Results for all three components are relative to the fixed reference. (d) Average $-\delta t/t$ over the frequency range 2-8 Hz (dotted lines) with one standard deviation (shaded areas). (e)-(h) Same as (a)-(d) for the moving reference approach.

0.15 (Fig. 2a-c), to focus on coda waves that are subject to seasonal variations. Fig. 3a-c shows that the seasonal pattern is most consistent for the lower frequencies, whereas above about 8 Hz, especially component EZ shows a different behaviour. Taking the average over the frequency range of 2-8 Hz (Fig. 3d) reveals a similar pattern for all three components with high velocities (high values in $-\delta t/t$) in the winter months and low velocities in the summer months. In addition, the time series exhibit a long-term velocity decrease.

To investigate potential artifacts due to cycle skipping when using the fixed reference, Fig. 3e-h shows the results for the moving reference approach (same processing otherwise). In this case, the seasonal pattern emerges more consistently over a broader frequency range, extending beyond 10 Hz. However, the 2-8 Hz averaged $-\delta t/t$ curves are similar as those for the fixed reference. While in the latter case, component EN is associated with an increased standard deviation (purple shading in Fig. 3d), using the moving reference results in increased uncertainty in component EZ. Regardless of the reference choice, the curves show the same characteristics, i.e. high (low) velocities in winter (summer) months and a long-term velocity decrease. However, careful inspection of Fig. 3e-g also reveals some high-velocity notches in summer, best visible on component EZ in 2011, 2012, 2013, and 2015 above 10 Hz. These features are also visible in Fig. 2d, where component EZ shows summer drops in $-\delta t/t$ that overshoot the lower cycle skipping limit and subsequently enter the plot again as steep lines from the upper cycle skipping limit. As using the moving reference (in 2016) does not eliminate this type of cycle skipping suggests that some years exhibit changes relative to 2016 that exceed the cycle skipping limit.

5 Discussion

5.1 Velocity changes

In most seismic monitoring applications, $-\delta t/t$ is obtained from linear regression assuming a bulk velocity change. Here, we find that only parts of the coda waves at different lag times show clear seasonal changes (Fig. 2a-c), which suggests localized changes and we consequently consider $-\delta t/t$ as a proxy for dv/v. To attach numbers to the seasonal and long-term changes, we fit a velocity change model consisting of the superposition of a sinusoid with a period of 365.25 d and a linear trend to the $-\delta t/t$ time series (eq (1), supporting information). Using the 2-8 Hz curves and averaging over the three components yields seasonal peak-to-peak velocity changes of 3.3% for the fixed reference and 2.9% for the moving reference and long-term velocity decreases of -0.14%/yr and -0.11%/yr, respectively. In addition to different reference approaches, we further examine different strategies in determining $-\delta t/t$ for component NZ (most consistent component), including linear regression analysis and the classical MWCS technique (see Text S2 for details). In all cases, we find seasonal velocity changes with high (low) values in late winter (summer) and a velocity decrease over the past 15 years. Yet, the amplitudes of both characteristics are smaller when using the whole coda wave window independent of the 365.25 d periodicity, which further supports that the velocity changes are localized. The observed 2-8 Hz velocity change characteristics appear to be present also at higher frequencies (Fig. 3), however, we refrain from analyzing a frequency dependence, as we are facing a complex setting with steep terrain and heterogeneously distributed medium changes, which is far off from a layered half space typically assumed e.g. in surface wave analysis (James et al., 2019). In addition, we encounter cycle skipping at higher frequencies, which partly remains even when using a moving reference. This suggests that large velocity changes (several percent) between the years are present, which is hardly explainable and may therefore also be an artefact of the year-by-year comparison of your moving reference approach.

The location of the velocity changes can be examined with travel time sensitivity kernels for a colocated source and receiver. In this case, the sensitivity kernels for both of the two end-member scenarios of single scattering (Pacheco & Snieder, 2006) and multiple scattering (Pacheco & Snieder, 2005) peak at the station location and decrease rapidly with distance from the station (Bennington et al., 2021; Sens-Schönfelder & Wegler, 2006). This implies that the velocity changes relate to the direct surroundings of the station (Hobiger et al., 2014) and we hypothesize that they are caused by thaw and refreeze associated with the permafrost lens documented in Krautblatter et al. (2010). The permafrost lens is separated by about 200 m from the station, which is only a fraction of one wavelength at the lowest frequencies considered. However, we also note that the single station sensitivity kernels may not comprehensively describe the encountered situation with a stationary noise source at the Zugspitze summit in some distance to the station. This situation also admits phases resulting from the cross-correlation of direct waves emitted from the noise source and their singly scattered (laterally or at depth) products, hence source and receiver being not colocated. This is expected to add travel time sensitivity also to the noise source region and the direct path between source and receiver (both of which are also affected by permafrost), similar as for two-station cross-correlation sensitivity kernels (Obermann et al., 2019). To further pinpoint the velocity changes, we note however, that denser instrumentation would be necessary.

5.2 Permafrost dynamics

We evaluate our hypothesis of freeze-thaw induced velocity changes by considering the recordings from a weather station at the Zugspitze summit run by the Deutscher Wetterdienst (DWD, German weather service). Fig. 4 shows the 2-8 Hz velocity changes (fixed reference, same as Fig. 3d), as well as the air temperature, snow height and fluid

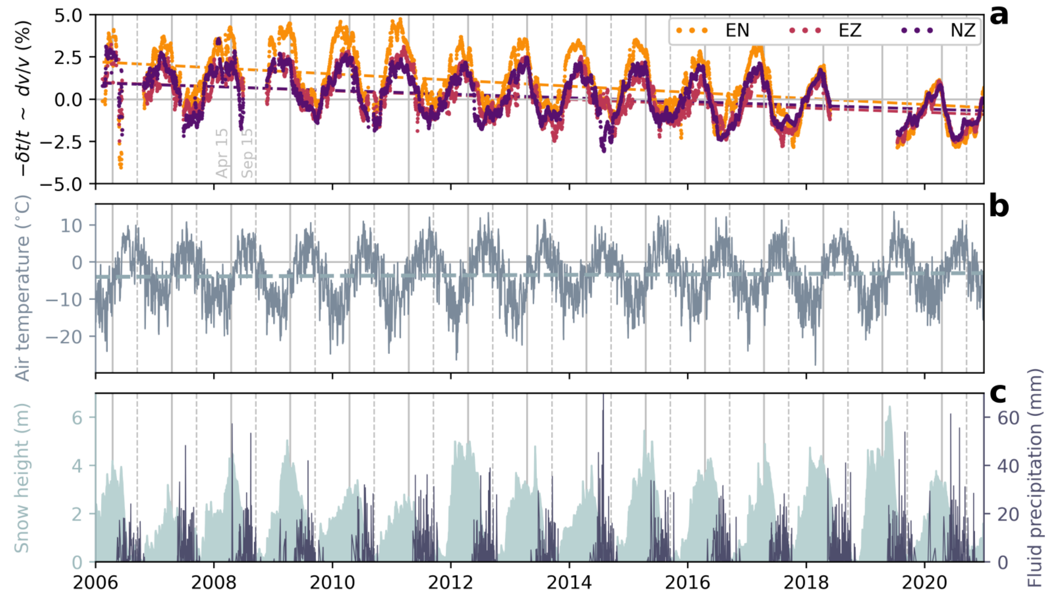

Figure 4. (a) 2-8 Hz velocity change (dotted lines, same as in Fig. 3d) and linear trend (dashed lines). Vertical solid and dashed lines indicate April 15 and September 15 of each year. (b) Daily mean air temperature (solid line) with linear trend (dashed line). (c) Snow height (greenish areas) and fluid precipitation (blueish bars). Time series in (b) and (c) are measured at the Zugspitze summit.

precipitation measured by the weather station. This reveals that the annual velocity drops starting in April (vertical gray solid lines) occur concurrently with air temperatures rising above the freezing point. This especially holds when adding an offset of around 1 °C to the temperature curve to account for the elevation difference between the summit and the ridge (assuming a atmospheric lapse rate of around -0.6 °C/100 m). Minimum annual velocities are reached in July and August, followed by a velocity increase starting in September, coincidentally with temperatures dropping below the freezing point (vertical gray dashed lines). With temperatures above the freezing point, the period between April and September, where the velocity decreases is furthermore characterized by snow melt and rain-dominated precipitation (Fig. 4c). Considering the long-term trend, the velocity drops on the order of 0.1 %/yr, while the temperature rises on average by 0.07 °C/yr in the time period between 2006-01-01 and 2021-01-01. The determined linear trends (using eq. (1), supporting information) are depicted by the colored dashed lines in Fig. 4a-b.

The permafrost lens in the ridge to the north of the seismic station (Fig. 1) is monitored by time-lapse temperature-calibrated ERT images (Scandroglio, Rehm, et al., 2021; Schroeder & Krautblatter, 2021), of which results are documented for 2007 (Krautblatter et al., 2010). (Krautblatter et al., 2010) observe pronounced melt from May to August with rock temperature changes being too fast to be solely explained by heat conduction. Coincidentally, they observe water seepage into the gallery and rapid melting along fracture zones suggesting warming and melting through water percolation. With temperatures dropping below the freezing point in September, the ERT results of Krautblatter et al. (2010) show refreezing from the rock face. Similar to the electrical resistivity, seismic velocities are different for frozen and unfrozen material and sharply increase at the freezing point (King et al., 1988; Leclaire et al., 1994; Kneisel et al., 2008). Laboratory experiments including samples from Mt. Zugspitze show that this also holds for low-porosity

Wetterstein limestones representative for the study site (Draebing & Krautblatter, 2012). The seasonal velocity changes can thus be explained by the annual heat wave causing progressive thawing to depth starting in spring from the rock face, which will decrease seismic velocities. The observed rapid decline of velocities is presumably enhanced by water percolation from melt and precipitation. Once temperatures drop again below the freezing point in fall, progressive refreezing from the rock face to depth will again increase the velocities. The immediate response of the velocity to the temperature dropping below and rising above the freezing point (fall and spring, respectively) appear plausible in the light that centimeter-scale ground freezing is sufficient to result in significant surface waves velocity changes (Steinmann et al., 2021). Finally, following the argumentation line from above, the long-term decrease in seismic velocities can be well explained by permafrost degradation, i.e. the shrinkage of the perennially frozen rock volume due to rising temperatures. This is also evident from borehole temperature logging beneath the summit (Gallemann et al., 2017).

6 Conclusions

Using passive seismic data from Mt. Zugspitze, we find seasonal seismic velocity changes as well as a velocity decrease over the observation period of 15 years. Comparison of our results with meteorological data and a previous ERT study suggest that these velocity changes are caused by seasonal freeze-thaw cycles and permafrost degradation, respectively. Although originally deployed for earthquake monitoring, we were able to exploit the seismic station for long-term permafrost monitoring yielding velocity change values on more than 80% of all days in the 15-year observation period. This highlights the cost and labour efficient potential of seismology for continuous permafrost monitoring, compared to other methods where long-term monitoring is challenged by manual data acquisition requiring regular field trips. Yet, the single station approach of this study is limited in the spatial resolution. Future studies should therefore extend the instrumentation in order to investigate permafrost dynamics with high spatio-temporal resolution. In this context, the recently introduced distributed acoustic sensing systems, which allow wave propagation sensing on a meter scale along fiber-optic cables are promising for detailed permafrost monitoring.

Acknowledgments

This study was financially supported by the Bayerisches Landesamt für Umwelt (LfU). We greatfully acknowledge support from the staff of the Schneefernerhaus for hosting the seismic station. Data of station BW.ZUGS is available through the EIDA node at http://erde.geophysik.uni-muenchen.de/fdsnws, data of the meteorological station through the DWD Climate Data Center (https://cdc.dwd.de/portal/, station ID 5792).

References

Becker, G., & Knapmeyer-Endrun, B. (2019). Crustal thickness from horizontal component seismic noise auto-and cross-correlations for stations in central and eastern europe. *Geophysical Journal International*, *218*(1), 429–445.

Beniston, M., Farinotti, D., Stoffel, M., Andreassen, L. M., Coppola, E., Eckert, N., … Vincent, C. (2018). The european mountain cryosphere: a review of its current state, trends, and future challenges. *The Cryosphere*, *12*(2), 759–794.

Bennington, N., Ohlendorf, S., Thurber, C., & Haney, M. (2021). Spatiotemporal analysis of seismic velocity changes at okmok volcano, alaska and implications from deformation source modeling. *Earth and Planetary Science Letters*, *561*, 116809.

Bensen, G., Ritzwoller, M., Barmin, M., Levshin, A. L., Lin, F., Moschetti, M., … Yang, Y. (2007). Processing seismic ambient noise data to obtain reliable broad-band surface wave dispersion measurements. *Geophysical Journal International*, *169*(3), 1239–1260.

Biskaborn, B. K., Smith, S. L., Noetzli, J., Matthes, H., Vieira, G., Streletskiy, D. A., ... Lantuit, H. (2019). Permafrost is warming at a global scale. *Nature communications*, *10*(1), 1–11.

Clarke, D., Zaccarelli, L., Shapiro, N., & Brenguier, F. (2011). Assessment of resolution and accuracy of the moving window cross spectral technique for monitoring crustal temporal variations using ambient seismic noise. *Geophysical Journal International*, *186*(2), 867–882.

Davies, M. C., Hamza, O., & Harris, C. (2001). The effect of rise in mean annual temperature on the stability of rock slopes containing ice-filled discontinuities. *Permafrost and periglacial processes*, *12*(1), 137–144.

Department of Earth and Environmental Sciences, Geophysical Observatory, LMU Munich. (2001). *BayernNetz [Data set].* International Federation of Digital Seismograph Networks. doi: 10.7914/SN/BW

De Plaen, R. S., Lecocq, T., Caudron, C., Ferrazzini, V., & Francis, O. (2016). Single-station monitoring of volcanoes using seismic ambient noise. *Geophysical Research Letters*, *43*(16), 8511–8518.

Draebing, D., & Krautblatter, M. (2012). P-wave velocity changes in freezing hard low-porosity rocks: a laboratory-based time-average model. *The Cryosphere*, *6*(5), 1163–1174.

Gallemann, T., Haas, U. H., Teipel, U., von Poschinger, A., Wagner, B., Mahr, M., & Bäse, F. (2017). Permafrost-Messstation am Zugspitzgipfel: Ergebnisse und Modellberechnungen. *Geologica Bavarica*, *115*, 1–77.

Gruber, S., & Haeberli, W. (2007). Permafrost in steep bedrock slopes and its temperature-related destabilization following climate change. *Journal of Geophysical Research: Earth Surface*, *112*(F2).

Gruber, S., Hoelzle, M., & Haeberli, W. (2004a). Permafrost thaw and destabilization of alpine rock walls in the hot summer of 2003. *Geophysical research letters*, *31*(13).

Gruber, S., Hoelzle, M., & Haeberli, W. (2004b). Rock-wall temperatures in the alps: modelling their topographic distribution and regional differences. *Permafrost and Periglacial Processes*, *15*(3), 299–307.

Gude, M., & Barsch, D. (2005). Assessment of geomorphic hazards in connection with permafrost occurrence in the Zugspitze area (Bavarian Alps, Germany). *Geomorphology*, *66*(1-4), 85–93.

Guillemot, A., Helmstetter, A., Larose, É., Baillet, L., Garambois, S., Mayoraz, R., & Delaloye, R. (2020). Seismic monitoring in the Gugla rock glacier (Switzerland): ambient noise correlation, microseismicity and modelling. *Geophysical Journal International*, *221*(3), 1719–1735.

Haeberli, W., Hoelzle, M., Kääb, A., Keller, F., Vonder Mühll, D., & Wagner, S. (1998). Ten years after drilling through the permafrost of the active rock glacier Murtèl, Eastern Swiss Alps: answered questions and new perspectives. In *Proceedings of the seventh international conference on permafrost* (pp. 403–410).

Haeberli, W., Noetzli, J., Arenson, L., Delaloye, R., Gärtner-Roer, I., Gruber, S., ... Phillips, M. (2010). Mountain permafrost: development and challenges of a young research field. *Journal of Glaciology*, *56*(200), 1043–1058.

Harris, C., & Cook, J. D. (1986). The detection of high altitude permafrost in jotunheimen, norway using seismic refraction techniques: an assessment. *Arctic and Alpine Research*, *18*(1), 19–26.

Hauck, C. (2002). Frozen ground monitoring using dc resistivity tomography. *Geophysical research letters*, *29*(21), 12–1.

Hauck, C. (2013). New concepts in geophysical surveying and data interpretation for permafrost terrain. *Permafrost and Periglacial Processes*, *24*(2), 131–137.

Hobiger, M., Wegler, U., Shiomi, K., & Nakahara, H. (2014). Single-station cross-correlation analysis of ambient seismic noise: application to stations in the surroundings of the 2008 Iwate-Miyagi Nairiku earthquake. *Geophysical Journal International*, *198*(1), 90–109.

Hoelzle, M., Mittaz, C., Etzelmüller, B., & Haeberli, W. (2001). Surface energy fluxes and distribution models of permafrost in European mountain areas: an overview of current developments. *Permafrost and Periglacial Processes*, *12*(1), 53–68.

Huggel, C., Allen, S., Deline, P., Fischer, L., Noetzli, J., & Ravanel, L. (2012). Ice thawing, mountains falling—are alpine rock slope failures increasing? *Geology Today*, *28*(3), 98–104.

James, S., Knox, H., Abbott, R., Panning, M., & Screaton, E. (2019). Insights into permafrost and seasonal active-layer dynamics from ambient seismic noise monitoring. *Journal of Geophysical Research: Earth Surface*, *124*(7), 1798–1816.

James, S., Knox, H., Abbott, R., & Screaton, E. (2017). Improved moving window cross-spectral analysis for resolving large temporal seismic velocity changes in permafrost. *Geophysical Research Letters*, *44*(9), 4018–4026.

Jerz, H., & von Poschinger, A. (1995). Neuere Ergebnisse zum Bergsturz Eibsee-Grainau. *Geologica Bavarica*(99), 383–398.

Jiang, C., & Denolle, M. A. (2020). Noisepy: A new high-performance python tool for ambient-noise seismology. *Seismological Research Letters*, *91*(3), 1853–1866.

Kane, D. L., Hinkel, K. M., Goering, D. J., Hinzman, L. D., & Outcalt, S. I. (2001). Non-conductive heat transfer associated with frozen soils. *Global and Planetary Change*, *29*(3-4), 275–292.

King, M. (1977). Acoustic velocities and electrical properties of frozen sandstones and shales. *Canadian Journal of Earth Sciences*, *14*(5), 1004–1013.

King, M., Zimmerman, R., & Corwin, R. (1988). Seismic and electrical properties of unconsolidated permafrost1. *Geophysical Prospecting*, *36*(4), 349–364.

Kneisel, C., Hauck, C., Fortier, R., & Moorman, B. (2008). Advances in geophysical methods for permafrost investigations. *Permafrost and periglacial processes*, *19*(2), 157–178.

Körner, H., & Ulrich, R. (1965). Geologische und felsmechanische Untersuchungen für die Gipfelstation der Seilbahn Eibsee–Zugspitze. *Geologica Bavarica*(55), 404–421.

Krautblatter, M., Funk, D., & Günzel, F. K. (2013). Why permafrost rocks become unstable: a rock–ice-mechanical model in time and space. *Earth Surface Processes and Landforms*, *38*(8), 876–887.

Krautblatter, M., & Hauck, C. (2007). Electrical resistivity tomography monitoring of permafrost in solid rock walls. *Journal of Geophysical Research: Earth Surface*, *112*(F2).

Krautblatter, M., Verleysdonk, S., Flores-Orozco, A., & Kemna, A. (2010). Temperature-calibrated imaging of seasonal changes in permafrost rock walls by quantitative electrical resistivity tomography (Zugspitze, German/Austrian Alps). *Journal of Geophysical Research: Earth Surface*, *115*(F2).

Leclaire, P., Cohen-Ténoudji, F., & Aguirre-Puente, J. (1994). Extension of Biot's theory of wave propagation to frozen porous media. *The Journal of the Acoustical Society of America*, *96*(6), 3753–3768.

Lecocq, T., Caudron, C., & Brenguier, F. (2014). Msnoise, a python package for monitoring seismic velocity changes using ambient seismic noise. *Seismological Research Letters*, *85*(3), 715–726.

Lomb, N. R. (1976). Least-squares frequency analysis of unequally spaced data. *Astrophysics and space science*, *39*(2), 447–462.

Mao, S., Mordret, A., Campillo, M., Fang, H., & van der Hilst, R. D. (2020). On the measurement of seismic traveltime changes in the time–frequency domain with wavelet cross-spectrum analysis. *Geophysical Journal International*, *221*(1), 550–568.

Mellor, M. (1973). Mechanical properties of rocks at low temperatures. In *2nd international conference on permafrost, yakutsk, international permafrost association* (pp. 334–344).

Mollaret, C., Hilbich, C., Pellet, C., Flores-Orozco, A., Delaloye, R., & Hauck, C. (2019). Mountain permafrost degradation documented through a network of permanent electrical resistivity tomography sites. *The Cryosphere*, *13*(10), 2557–2578.

Noetzli, J., & Gruber, S. (2009). Transient thermal effects in Alpine permafrost. *The Cryosphere*, *3*(1), 85–99.

Nötzli, J., Gruber, S., & Poschinger, A. v. (2010). Modellierung und Messung von Permafrosttemperaturen im Gipfelgrat der Zugspitze, Deutschland. *Geographica Helvetica*, *65*(2), 113–123.

Obermann, A., Planès, T., Larose, E., & Campillo, M. (2019). 4-D Imaging of Subsurface Changes with Coda Waves: Numerical Studies of 3-D Combined Sensitivity Kernels and Applications to the Mw 7.9, 2008 Wenchuan Earthquake. *Pure and Applied Geophysics*, *176*(3), 1243–1254.

Pacheco, C., & Snieder, R. (2005). Time-lapse travel time change of multiply scattered acoustic waves. *The Journal of the Acoustical Society of America*, *118*(3), 1300–1310.

Pacheco, C., & Snieder, R. (2006). Time-lapse traveltime change of singly scattered acoustic waves. *Geophysical Journal International*, *165*(2), 485–500.

Phillips, M., Wolter, A., Lüthi, R., Amann, F., Kenner, R., & Bühler, Y. (2017). Rock slope failure in a recently deglaciated permafrost rock wall at Piz Kesch (Eastern Swiss Alps), February 2014. *Earth Surface Processes and Landforms*, *42*(3), 426–438.

Pirulli, M. (2009). The Thurwieser rock avalanche (Italian Alps): Description and dynamic analysis. *Engineering Geology*, *109*(1-2), 80–92.

Ravanel, L., Magnin, F., & Deline, P. (2017). Impacts of the 2003 and 2015 summer heatwaves on permafrost-affected rock-walls in the Mont Blanc massif. *Science of the Total Environment*, *609*, 132–143.

Scandroglio, R., Draebing, D., Offer, M., & Krautblatter, M. (2021). 4D quantification of alpine permafrost degradation in steep rock walls using a laboratory-calibrated electrical resistivity tomography approach. *Near Surface Geophysics*, *19*(Near-Surface Geophysics for Geohazard Assessment), 241–260.

Scandroglio, R., Rehm, T., Limbrock, J. K., Kemna, A., Heinze, M., Pail, R., & Krautblatter, M. (2021). *Decennial multi-approach monitoring of thermo-hydro-mechanical processes, Kammstollen outdoor laboratory, Zugspitze (Germany).* EGU General Assembly 2021, online, 19–30 Apr 2021. doi: https://doi.org/10.5194/egusphere-egu21-13815

Scargle, J. D. (1982). Studies in astronomical time series analysis. ii-statistical aspects of spectral analysis of unevenly spaced data. *The Astrophysical Journal*, *263*, 835–853.

Schroeder, T., & Krautblatter, M. (2021). *A high-resolution multi-phase thermo-geophysical permafrost rock model to verify long-term ERT monitoring at the Zugspitze (German/Austrian Alps).* EGU General Assembly 2021, online, 19–30 Apr 2021. doi: https://doi.org/10.5194/egusphere-egu21-15231

Sens-Schönfelder, C., & Wegler, U. (2006). Passive image interferometry and seasonal variations of seismic velocities at Merapi Volcano, Indonesia. *Geophysical research letters*, *33*(21).

Steinmann, R., Hadziioannou, C., & Larose, E. (2021). Effect of centimetric freezing of the near subsurface on Rayleigh and Love wave velocity in ambient seismic noise correlations. *Geophysical Journal International*, *224*(1), 626–636.

Timur, A. (1968). Velocity of compressional waves in porous media at permafrost temperatures. *Geophysics*, *33*(4), 584–595.

Ulrich, R., & King, L. (1993). Influence of mountain permafrost on construction in the Zugspitze mountains, Bavarian Alps, Germany. In *Proceedings of the Sixth Internatinnal Conference on Permafrost, Beijing* (pp. 625–630).

Walter, F., Amann, F., Kos, A., Kenner, R., Phillips, M., de Preux, A., . . . Yves (2020). Direct observations of a three million cubic meter rock-slope collapse with almost immediate initiation of ensuing debris flows. *Geomorphology*, *351*, 106933.

Yates, A., Savage, M., Jolly, A., Caudron, C., & Hamling, I. (2019). Volcanic, coseismic, and seasonal changes detected at White Island (Whakaari) volcano, New Zealand, using seismic ambient noise. *Geophysical Research Letters*, *46*(1), 99–108.

Zhang, T., Barry, R., Knowles, K., Heginbottom, J., & Brown, J. (2008). Statistics and characteristics of permafrost and ground-ice distribution in the Northern Hemisphere. *Polar Geography*, *31*(1-2), 47–68.

Supporting Information for "Seasonal freeze-thaw cycles and permafrost degradation on Mt. Zugspitze (German/Austrian Alps) revealed by single-station seismic monitoring"

Fabian Lindner[1], Joachim Wassermann[1], Heiner Igel[1]

[1]Department of Earth and Environmental Sciences, LMU Munich, Theresienstraße 41, 80333, Munich, Germany

Contents of this file

Text S1: Moving reference approach

To extract travel time shifts, time-lapse cross-correlations are compared to a reference cross-correlation. If travel time shifts change smoothly but reach large values relative to the reference period such that cycle skipping occurs, one may compare cross-correlations from adjacent dates (e.g. this week versus last week), assuming small velocity changes between the dates. This is relevant for permafrost monitoring, as thaw and refreeze can be

---

associated with such strong velocity changes, that the measurement of travel time shifts is affected by cycle skipping (James et al., 2017, 2019). We therefore also determine travel time shifts using a moving reference similar as in James et al. (2017), in addition to the fixed reference approach. Here, we are dealing with smooth seasonal velocity changes, which we determine in a first step with a moving approach for 2016 (no gaps and no changes in instrumentation): For each 15 d moving stack in 2016, we determine $\delta t(t, f)$ relative to the previous, neighbouring 15 d stack that is not overlapping with the current stack (e.g. 2016-02-01 serves as reference for 2016-02-16). In case the reference dates back to 2015, we take 2016-01-01 as reference (e.g. 2016-01-01 serves as reference for 2016-01-05). To obtain meaningful time series, we then accumulate the travel time shifts from neighbouring 15 d stacks, e.g. for 2016-02-26 we sum up the values obtained for 2016-01-12 (relative to 2016-01-01), 2016-01-27, and 2016-02-11. Thereby, we strictly speaking end up with 15 time series relative to 2016-01-01, together building the seasonal cycle for 2016. In the second step, we determine all deviations from this cycle: for each 15 d stack outside 2016, we calculate $\delta t(t, f)$ relative to the respective date in 2016, e.g. for 2007-08-19 we use 2016-08-19 as reference, and sum up the travel time shifts of both dates.

The described procedure assumes a periodic velocity change cycle with similar velocity changes at the same date at different years. In summary, we first determine the variations in 2016 and subsequently the changes relative to 2016, hence cycle skipping should be eliminated for smooth travel time changes with a periodicity of one year. This strategy further keeps the number of summations and thus the error propagation at a moderate level compared to using a moving reference for the complete data set of 15 years. Furthermore, the latter can hardly be applied, as data gaps prevent the continuous travel time tracking, resulting in erroneous offsets.

Text S2: Velocity change results obtained from different approaches

In most applications, $-\delta t/t$ is obtained from linear regression using travel time shifts δt at different lag times t and the results are typically interpreted as velocity change dv/v, which is exact in the case of a bulk velocity change affecting the whole medium of consideration. In this study, we used only specific parts of the cross-correlation showing high 365.25 d periodicity and determined $-\delta t/t$ as the median from individual $-\delta t/t$ curves for each frequency bin. In this section, we examine different scenarios for the $-\delta t/t$ extraction including linear regression for each frequency bin and the classical moving-window cross-spectral (MWCS) technique. To facilitate the comparison of the different approaches, we determine the key quantities, i.e. the seasonal velocity change and the long-term velocity change, by fitting a model consisting of the superposition of a sinusoid and a linear trend to the $-\delta t/t$ time series, i.e.

$$\Delta_m = c_1 \cos(2\pi f_{yr} t_{UTC}) + c_2 \sin(2\pi f_{yr} t_{UTC}) + c_3 \, t_{UTC} + c_4, \tag{1}$$

where f_{yr} is the frequency of one year, i.e. the inverse of 365.25 d, and t_{UTC} refers to the absolute time. Employing linear least squares to fit the model to the data, we obtain the constants c_1 to c_4, which we use to calculate the seasonal peak-to-peak velocity change given by $2\sqrt{c_1^2 + c_2^2}$. In addition, c_3 yields the slope, i.e. the linear trend. Furthermore, one may calculate the phase of the sinusoid given by $arctan2(c_2/c_1)$, which can be used to determine the timing of the seasonal maxima and minima of the sinusoid.

Because component NZ yields the most consistent results between 2 and 8 Hz for both the fixed and the moving reference (smaller standard deviation than EN and EZ components), we focus the comparison on this component and frequency range. Fig. S1a (black line) shows the NZ $-\delta t/t$ curve from Fig. 3d (main manuscript) relative to the fixed reference, i.e. the median $-\delta t/t$ curve for each frequency bin considering only those that show a normalized Lomb-Scargle amplitude of at least 0.15 and subsequently averaged over 2-8 Hz. Furthermore, Fig. S1a shows the model fit (eq. 1) to this curve (orange dashed line). The corresponding peak-to-peak amplitude of seasonal velocity changes exceeds 3% and the velocity decreases on average by about 0.11 %/yr (scenario 1 in Fig. S1b). Similar results are obtained when using the moving reference (3.7% peak-to-peak and -0.08 %/yr, scenario 2). Next, we also consider the common approach of using a linear regression (here without applying weights) at each time step to determine a $-\delta t/t$ time series for each frequency bin (using again one and 15 periods as lag time limits). We use the fixed reference and consider only those lag times with $A_{LS}(365.25d) \geq 0.15$ (scenario 3) and regardless of $A_{LS}(365.25d)$ (i.e. using all δt values in the considered lag range, scenario 4). For the 2-8 Hz averaged results, we obtain peak-to-peak amplitudes of 2.5 % and 0.9 % (scenarios 3 and 4, respectively) and long-term velocity decreases of -0.085 %/yr and -0.04%/yr. Finally, we consider the $-\delta t/t$ curve obtained from the widely used MWCS analysis in the lag and frequency range of 0.5-4 s and 2-8 Hz, respectively (scenario 5). Within the lag window, we use a moving window of 0.75 s width with overlap of 0.5 s to determine the frequency-averaged travel time shifts as a function of lag time, which we subsequently use in a linear regression to determine $-\delta t/t$. The resulting velocity changes and the corresponding model fit are shown in Fig. S1a (grey and red line, respectively). Also here, we find a seasonal velocity variation with peak-to-peak amplitude of 1 % and a velocity decrease of -0.01 %/yr. However, we note that when using MWCS, only component NZ shows clear seasonal velocity variations. With regard to the phase of the seasonal velocity changes, all scenarios yield delays ranging between 50 and 60 d, meaning that the annual maximum of the sinusoid model is reached in late February to early March. While all approaches yield a similar velocity change pattern, the velocity change amplitudes are dependent on the processing and the selected coda wave windows.

References

James, S., Knox, H., Abbott, R., Panning, M., & Screaton, E. (2019). Insights into permafrost and seasonal active-layer dynamics from ambient seismic noise monitoring. *Journal of Geophysical Research: Earth Surface*, *124*(7), 1798–1816.

James, S., Knox, H., Abbott, R., & Screaton, E. (2017). Improved moving window cross-spectral analysis for resolving large temporal seismic velocity changes in permafrost. *Geophysical Research Letters*, *44*(9), 4018–4026.

Lecocq, T., Caudron, C., & Brenguier, F. (2014). Msnoise, a python package for monitoring seismic velocity changes using ambient seismic noise. *Seismological Research Letters*, *85*(3), 715–726.

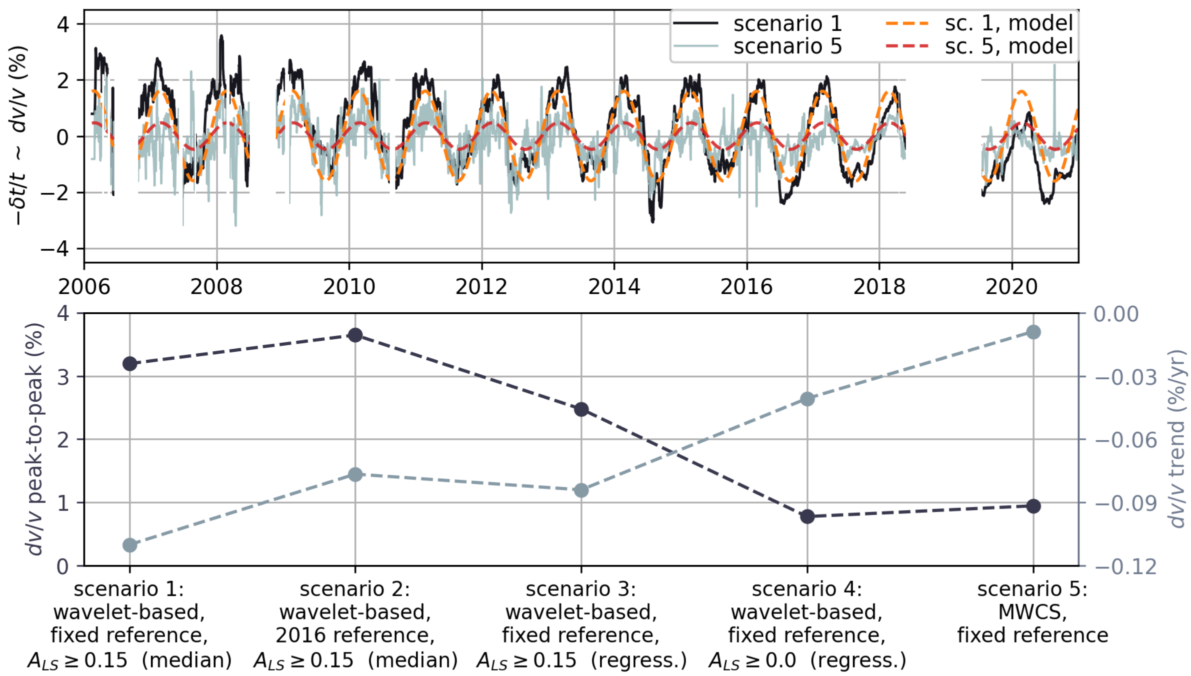

Figure S1. Comparison of different approaches to extract velocity changes from component NZ. (a) Velocity change relative to the fixed reference by calculating the median of travel time change curves associated with high 365.25 d periodicity ($A_{LS} \geq 0.15$) in each frequency bin and averaging over 2-8 Hz (black line, scenario 1; same as in Fig. 3d, main manuscript). Also shown is the velocity change relative to the fixed reference obtained from classical MWCS analysis in the frequency range 2-8 Hz (gray line, scenario 5). The orange and red dashed lines depict the velocity change model (eq. 1) fits to the two time series (scenario 1 and 5, respectively). (b) Seasonal velocity change peak-to-peak amplitude and long-term velocity change obtained by fitting the model from eq. (1) to the different velocity change time series (scenarios 1 to 5, see text for details).

Config parameter	Value
startdate	2006-01-01
enddate	2021-01-01
analysis_duration	86400
cc_sampling_rate	100.0
resampling_method	Lanczos
preprocess_lowpass	25.0
preprocess_highpass	0.01
preprocess_max_gap	10.0
preprocess_taper_length	20.0
remove_response	Y
response_format	inventory
response_prefilt	(0.005, 0.006, 30.0, 35.0)
maxlag	15.0
corr_duration	1800.0
overlap	0.0
windsorizing	3
whitening	A
whitening_type	B
stack_method	linear
cc_type	CC
components_to_compute_single_station	EN,EZ,NZ
ref_begin	2017-09-01
ref_end	2018-05-01
mov_stack	15
Filter parameter	
Low	0.1
High	25.0

Table S1. MSNoise (Lecocq et al., 2014) processing parameters used for the calculation of the single-station cross-correlations of station BW.ZUGS.